Perovskite solar cell developments, what's next?

Fu, Qiang; Jen, Alex K.Y.

Published in:
Next Energy

Published: 01/03/2023

Document Version:
Final Published version, also known as Publisher's PDF, Publisher's Final version or Version of Record

Published version (DOI):
10.1016/j.nxener.2023.100004

Publication details:
Fu, Q., & Jen, A. K. Y. (2023). Perovskite solar cell developments, what's next? *Next Energy*, *1*(1), Article 100004. https://doi.org/10.1016/j.nxener.2023.100004

All-Optical Tunable Filter With a Graphene-Buried Long-Period Waveguide Grating

Lianzhong Jiang, Wenfan Jiang, and Kin Seng Chiang, *Senior Member, IEEE*

***Abstract*—We demonstrate low-power all-optical tunable filters with long-period gratings formed in graphene-buried polymer waveguides, where the heat generated by graphene's absorption of the TE-polarized pump light serves to tune the TM-polarized resonance band. Our experimental gratings designed for operation at ∼1550 nm and pumped at 980 nm, which contain ∼6-mm long graphene, achieve a tuning efficiency of approximately –0.7 nm/mW, which corresponds to a ∼20-nm blue shift in the resonance wavelength with a pump power lower than ∼30 mW. Our grating can also serve as an all-optical switch when operated at a fixed wavelength, which can provide an extinction ratio larger than 20 dB with a pump power lower than 30 mW at a response time of ∼2.0 ms. The graphene-buried grating platform can be further explored for the development of a wide range of all-optical control devices.**

***Index Terms*—All-optical tunable filter, graphene, long-period grating, polymer waveguide.**

I. Introduction

ALL-OPTICAL tunable filters, whose transmission spectra can be tuned by control pump light, can find promising applications in optical signal processing [1]. Recently, graphene's photothermal effect has been explored for the realization of all-optical tunable filters, where a fiber or waveguide resonator, such as a microring [2], [3], [4] or a nanobeam cavity [5], is covered with graphene for pump absorption. All these devices are narrow-band filters formed on high-index-contrast waveguides or fibers, where the graphene film strongly absorbs both the pump light and the signal light [2], [3], [4], [5]. To keep the signal loss small, a short graphene length must be used and the tuning efficiency is compromised. The highest tuning efficiency of 216 pm/mW is achieved with an Si microring covered with a 5-μm-long graphene film, which induces a signal loss of 0.1 dB/μm [2]. In this article, we propose an all-optical tunable broadband filter based on the structure of a long-period waveguide grating (LPWG) formed in a graphene-buried polymer waveguide. Our device can provide high tuning efficiency, low pump power consumption, and low graphene-induced signal loss.

An LPWG is a periodic structure formed along an optical planar waveguide, which is originally proposed for achieving power transfer between a guided core mode and a cladding mode at a specific resonance wavelength [6]. While an LPWG is intrinsically a broadband rejection filter [6], [7], [8], the grating structure is so flexible that it has been applied to the development of a wide range of devices on different waveguide platforms, such as band-pass filters [9], wavelength add-drop multiplexers [10], mode converters [11], polarizers [12], spot-size converters [13], and mode switches [14], [15]. There have also been attempts to achieve all-optical switching with nonlinear long-period gratings based on the Kerr effect in silica [16] and chalcogenide [17] fibers, but the Kerr effect is so weak that the gratings must be operated with high pump powers that can only be delivered with expensive pulse lasers. Our proposed graphene-buried waveguide grating, however, can operate at low pump powers generated from low-cost continuous-wave (CW) lasers.

Graphene-buried polymer waveguides have been explored for the realization of passive and active devices, such as polarizers [18], [19], mode filters [19], [20], mode switches [21], and optical loss modulators [22]. Recently, we have shown that a graphene-buried polymer waveguide can be a highly efficient platform for the application of graphene's photothermal effect [23], [24]. Thanks to the fact that graphene strongly absorbs the electric field in parallel with its surface and does not absorb the electric field perpendicular to its surface [18], we can design a graphene-buried polymer waveguide to operate for the TM polarization (whose major electric-field component is perpendicular to the graphene surface) with negligible loss, while utilizing the large absorption of the TE polarization (whose major electric-field component is in parallel with the graphene surface) to generate heat [23], [24]. Such a feature is not available with high-index-contrast waveguides like silicon waveguides, where the modes are not linearly polarized. In addition, the polymer waveguide technology allows graphene to be placed near the waveguide core to facilitate heat transfer [21] and the large thermo-optic coefficient of the polymer material can further reduce the pump power required. The fiber-coupling losses for polymer waveguides are also low. All these advantages associated with the graphene-buried polymer waveguide platform can facilitate the realization of low-power all-optical control devices. In this study, we apply this platform to the achievement of a new function, namely all-optical wavelength tuning, and evaluate its performance. Our experimental LPWGs, which are designed for operation at ∼1550 nm for the TM polarization, can be tuned over a wavelength range of ∼20 nm (approximately the bandwidth of the rejection band) with a TE-polarized 980-nm

Manuscript received 3 April 2023; revised 5 June 2023; accepted 26 June 2023. Date of publication 30 June 2023; date of current version 10 July 2023. This work was supported by the Research Grants Council, University Grants Committee (RGC, UGC), Hong Kong, CityU 11212621. *(Corresponding author: Kin Seng Chiang.)*

The authors are with the Department of Electrical Engineering, City University of Hong Kong, Hong Kong, China (e-mail: lianjiang9-c@my.cityu.edu.hk; wenfjiang2-c@my.cityu.edu.hk; eeksc@cityu.edu.hk).

Digital Object Identifier 10.1109/JPHOT.2023.3290921

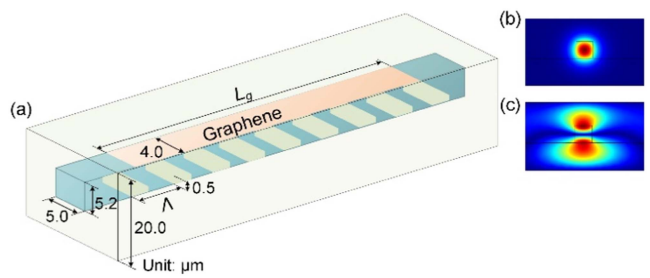

Fig. 1. (a) Schematic diagram showing the structure of the proposed graphene-buried LPWG and intensity profiles of the two coupled modes calculated at 1550 nm for our polymer waveguide: (b) the TM_{00} core mode and (c) the TM_{01} cladding mode.

pump power lower than ∼30 mW. When operated at a fixed signal wavelength, our LPWG can also function as an all-optical switch. Our typical switch can provide an extinction ratio higher than 20 dB with a pump power lower than 30 mW at a response time of ∼2.0 ms. Our device is suitable for applications where high-speed operation is not required (such as circuit switching), but low-power activation with CW lasers is important [1].

II. Operation Principle and Design

Fig. 1(a) shows the structure of our polymer waveguide device, where a corrugated grating of length L_g is formed at the bottom of the core and a graphene film of the same length is placed on the core right above the grating. The core supports only a single mode, while the cladding supports a number of cladding modes. The grating is designed for coupling between the core mode and the lowest-order cladding mode, whose intensity profiles for the TM polarization are shown in Fig. 1(b) and (c), respectively. Given the waveguide dimensions, the grating pitch Λ can be determined from the phase-matching condition [6]:

$$\Lambda = \frac{\lambda}{N_0 - N_1} \tag{1}$$

where λ is the resonance wavelength and N_0 and N_1 are the effective indices of the core mode and the cladding mode, respectively. The coupling efficiency of the grating is governed by the coupling coefficient κ, which is a measure of the spatial overlap between the two modes in the corrugated area [6]:

$$\kappa = \frac{\omega_0 \varepsilon_0 \left(n_{co}^2 - n_{cl}^2\right)}{4} \iint_S E_1 E_2 dS \tag{2}$$

where ω_0 is the angular optical frequency at the resonance wavelength, ε_0 is the permittivity of vacuum, n_{co} and n_{cl} are the refractive indices of the core and the cladding, respectively, E_1 and E_2 are the normalized electric fields of the core mode and the cladding mode, respectively, and S denotes the corrugated area. To achieve a 100% coupling efficiency at the resonance wavelength, the condition $\kappa L_g = \pi/2$ must be satisfied, from which we can determine the corrugation depth and the grating length required.

For the device to operate as an all-optical tunable filter, both signal light and pump light are launched into the waveguide. The heat generated from the absorption of the pump light by graphene increases the temperature of the grating. As the graphene film is placed on the core, the core mode experiences a larger average temperature change than the cladding mode. As a result, the effective-index difference $N_0 - N_1$ changes with the pump power, which thus gives rise to a shift in the resonance wavelength. To maximize pump absorption (i.e., minimize the pump power) and minimize signal absorption, the pump light is TE-polarized and the signal light is TM-polarized. There is no restriction on the pump wavelength, as long as it is outside the resonance band of the grating. In our study, we choose 980 nm as the pump wavelength for convenience.

The polymer materials for the core and the cladding are EpoCore and EpoClad (Micro Resist Technology), respectively [18], [19], [20], [21], [22], [23], [24], [25], whose refractive indices measured at 1530 nm are $n_{co} = 1.569$ and $n_{cl} = 1.560$, respectively. The grating is formed on a SiO_2-Si substrate with a SiO_2 layer of 5.0 μm. We employ a commercial mode solver (COMSOL) based on the full-vector finite-element method to calculate the variations of the effective indices of the modes with the waveguide dimensions, from which we can determine the core dimensions that support only the fundamental TE_{00} and TM_{00} modes. As shown in Fig. 1(a), the waveguide used in our study has a core with a size of 5.0 μm × 5.2 μm and a cladding with a thickness of 20.0 μm. The near-square core design can help to reduce the fiber-waveguide coupling loss. At 1550 nm, the effective indices of the two lowest-order TM modes, i.e., the TM_{00} and TM_{01} modes, are $N_0 = 1.5634$ and $N_1 = 1.5586$, respectively, which confirms that the TM_{00} mode (with $n_{cl} < N_0 < n_{co}$) is a core mode and the TM_{01} mode (with $N_1 < n_{cl}$) is a cladding mode. Because the index difference between the core and the cladding is small, the TE mode and the TM mode of the same order are almost degenerate. We calculate the values of N_0 and N_1 at different wavelengths and show the variation of the resonance wavelength with the grating pitch (the phase-matching curve) in Fig. 2(a) for both TE and TM polarizations. As shown in Fig. 2(a), the phase-matching condition is polarization-insensitive. The graphene film, which is placed symmetrically on the core, has a width of 4.0 μm. With these parameters, we calculate the graphene-induced losses by applying the interface model of graphene, whose complex conductivities are $6.084 \times 10^{-5} - 1.596 \times 10^{-6} i$ and $6.079 \times 10^{-5} - 8.616 \times 10^{-6} i$ for 980 nm and 1550 nm, respectively [18]. The calculated graphene-induced losses to the TE core mode are 26.8 dB/cm at 980 nm and 35.1 dB/cm at 1550 nm, while those to the TM core mode are 0.26 dB/cm at 980 nm and 0.25 dB/cm at 1550 nm. The absorption loss for the TE polarization is much larger than that of the TM polarization. With the effective indices and the mode fields obtained from the mode solver, we calculate the coupling coefficient κ as a function of the corrugation depth from (2) for a grating with a resonance wavelength of 1550 nm, from which we determine the variations of the grating length $L_g = \pi/(2\kappa)$ and the 3-dB bandwidth of the rejection band [26] with the corrugation depth. As shown in Fig. 2(b), as the corrugation depth increases, the grating length L_g decreases, while the 3-dB bandwidth increases. To achieve a high tuning efficiency, we should use a sufficiently long graphene film for

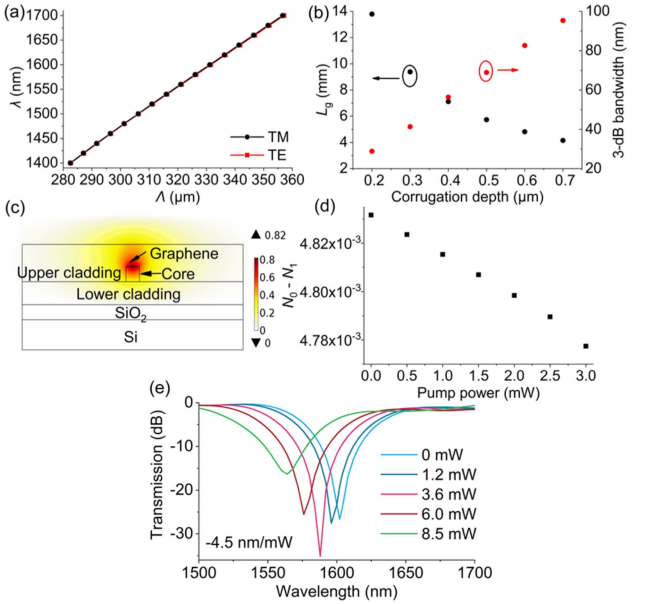

Fig. 2. (a) Phase-matching curves for the TM and TE polarizations; (b) varaiations of the grating length L_g and the 3-dB bandwidth with the corrugation depth for a grating with a resonance wavelength of 1550 nm; (c) temperature distribution of the waveguide calculated for a pump power of 1.0 mW; (d) variation of the effective-index difference with the pump power calculated at 1550 nm for the TM polarization; and (e) TM-polarized transmission spectra calculated at different pump powers for a grating with a pitch of $\Lambda = 332$ μm.

pump absorption, i.e., a sufficiently long grating. In our design, we choose a corrugation depth of 0.50 μm, which gives a grating length of 5.7 mm and a 3-dB bandwidth of ~69 nm.

To calculate the tuning efficiency, we treat the graphene as a heater that generates heat from the absorbed pump power. To simplify our analysis, we assume that all the pump light absorbed is converted into heat and, because of the very high thermal conductivity of graphene (~5000 W/m·K [23]), the heat is distributed evenly on the graphene film. We then employ the heat transfer module in COMSOL to simulate the temperature distribution by modelling graphene as a heat source without thickness, where the thermal conductivities of the polymer material, SiO_2, and Si are set at 0.12, 1.38, and 130 W/m·K, respectively. As shown in Fig. 2(c), the graphene heater raises the temperature of the core to a maximum value of 0.82 K for a 1-mW pump power. Knowing the temperature distribution, we can obtain the refractive-index distribution by assuming a thermo-optic coefficient of -1.0×10^{-4} for the polymer material and calculate the changes in the values of N_0 and N_1. For 1-mW pump power, N_0 and N_1 change by -4.74×10^{-5} and -2.97×10^{-5}, respectively. As a result, the effective-index difference $N_0 - N_1$ decreases with an increase in the pump power, as shown in Fig. 2(d). As an example, we calculate the transmission spectra of a grating with a pitch of $\Lambda = 332$ μm and a length of 18 periods at different pump powers for the TM polarization by using a 3D finite-difference beam propagation method (BPM) (3DFD-BPM, RSoft). The results are shown in Fig. 2(e). As shown in Fig. 2(e), the resonance wavelength can be tuned by 38 nm from 1602 nm to 1564 nm by increasing the pump power from 0 mW to 8.5 mW, which corresponds to a tuning efficiency

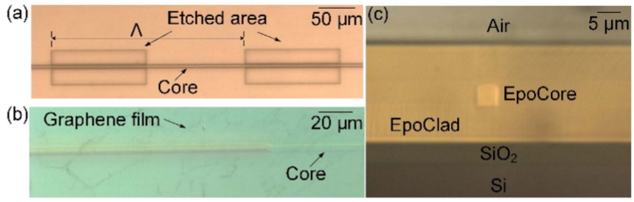

Fig. 3. Microscopic images showing (a) a waveguide core formed on an etched grating, (b) a graphene film placed on the sample with the strip on the core covered by photoresist, and (c) an end face of a fabricated waveguide.

of –4.5 nm/mW. The contrast of the resonance dip varies slightly with the pump power, because of the small changes in the coupling coefficient. The grating can also function as an all-optical switch when operating at a specific wavelength. For the grating with a pitch of 332 μm, if the signal wavelength is set at 1602 nm, the signal can be switched on and off with an extinction ratio of 23.2 dB by switching the pump power between 0 mW and 8.5 mW.

III. Fabrication Process

We fabricated the device with our in-house microfabrication facilities [18], [19], [20], [21], [22], [23], [24], [25]. First, a 7.7-μm EpoClad film was spin-coated on a SiO_2-Si substrate (which had a 5.0-μm thick SiO_2 layer) as the lower cladding. The grating with a corrugation depth of ~0.5 μm and a length of ~6 mm was formed on the lower cladding by photolithography and reactive ion etching (RIE). An EpoCore film with a thickness of ~5.0 μm was then spin-coated on the lower cladding and etched into a core by photolithography and wet-etching. A microscopic image of the etched area together with the core is shown in Fig. 3(a). An EpoClad film slightly thicker than the core layer was spin-coated onto the sample as the mid-cladding, which was etched down to the core by RIE to form a flat surface for graphene transfer. The RIE process also allowed the thickness of the core layer to be trimmed to the desired value. A commercial monolayer graphene film with a polymethyl-methacrylate (PMMA) buffer (Hefei Vigon Material Technology) was wet-transferred onto the sample, and the PMMA buffer was then removed by acetone. The graphene film was next patterned into a strip aligned with the grating by photolithography and O_2 RIE. A microscopic image of the graphene-covered waveguide is shown in Fig. 3(b), where the graphene strip on the core is coated with photoresist. Finally, an 8.0-μm EpoClad film was spin-coated onto the sample as the upper cladding. Fig. 3(c) shows an end face of the fabricated waveguide. The total length of the waveguide was ~9 mm. We actually fabricated a large number of gratings with different pitches, as well as reference waveguides (i.e., waveguides without gratings) with and without graphene on the same chip to facilitate device characterization. In our fabrication process, the uncertainties in the control of the etching depth, the core width, and the core height are about ± 0.1 μm, ± 0.3 μm, and ± 0.1 μm, respectively. While the fabrication errors affect the accuracy in the control of the transmission characteristics of the grating, especially the resonance wavelength,

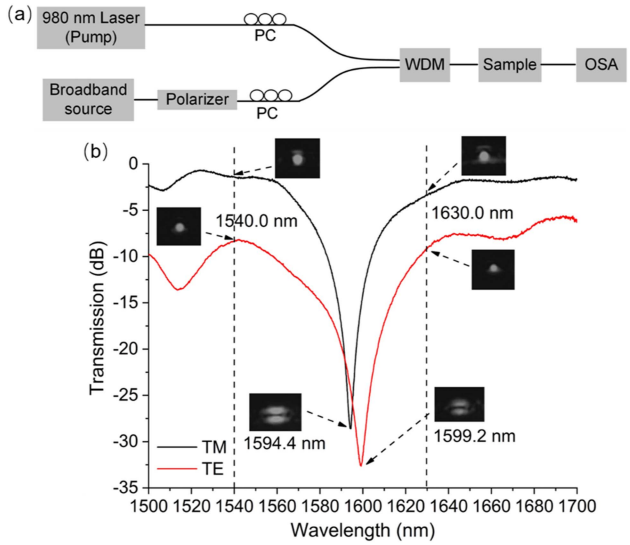

Fig. 4. (a) Experimental setup for grating characterization; (b) normalized transmission spectra measured for a graphene-buried grating with a pitch of $\Lambda = 332$ μm for the TM and TE polarizations when the pump is off, together with output near-field images taken at different wavelengths.

thermal tuning and, in fact, the all-optical tuning itself can, to a large extent, relax the fabrication tolerances.

IV. Experimental Results

A. Transmission Spectra and Loss Measurement

Fig. 4(a) shows a schematic diagram of the experimental setup for the characterization of our all-optical tunable filter. We first measured the transmission spectrum (at 25 °C) of a device under test by launching light from a broadband source (LEUKOS, Samba) into the waveguide with a single-mode fiber (SMF) when the pump light was turned off. The polarization state of the broadband source was controlled by a fiber polarizer and a polarization controller (PC). We used another SMF to collect the light from the output end and measured the spectrum with an optical spectrum analyzer (OSA) (Agilent, 86140B). We carefully adjusted the fiber-waveguide coupling to ensure that only the core mode was launched and detected. The spectrum was normalized with that from a reference waveguide without graphene. Fig. 4(b) shows the normalized TE and TM transmission spectra of a typical fabricated grating, which has a pitch of 332 μm. The resonance wavelength is 1594.4 nm (1599.2 nm) for the TM (TE) polarization, which is close to the simulation value 1602 nm (1601 nm). The discrepancies can be attributed to errors in the refractive indices of the materials and the fabrication process. The contrast at the resonance wavelength is larger than 20 dB for both polarizations, which corresponds to a coupling efficiency larger than 99%. The 3-dB bandwidth of the rejection band is ~62 nm for the TM polarization, which agrees well with the simulation result (~69 nm). As shown in Fig. 4(b), the off-resonance background transmission of the TM polarization is about –0.6 dB, which implies negligible graphene-induces loss. On the other hand, the off-resonance background transmission of the TE polarization is much weaker. By measuring the insertion

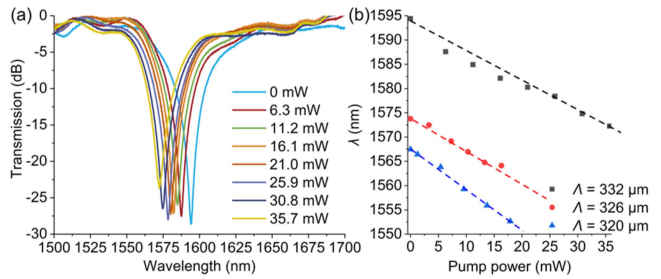

Fig. 5. (a) TM-polarized normalized transmission spectra of a graphene-buried grating with $\Lambda = 332$ μm measured at different pump powers, and (b) variation of the resonance wavelength with the pump power for three gratings with different pitches.

losses of several reference waveguides with graphene for both polarizations, we estimated that the graphene induced loss for the TE core mode was within 7.2 – 9.6 dB/cm at 1550 nm. The measured value is significantly smaller than the theoretical value, which, we believe, is caused by the presence of cracks and holes on the graphene film, as shown in Fig. 3(b). We also took output near-field images at different wavelengths with a tunable laser (Keysight, 8163B) and an infrared camera (Hamamatsu, C2714), and display the images in Fig. 4(b). These images confirm strong coupling between the core mode and the desired cladding mode at the resonance wavelength.

B. All-Optical Wavelength Tuning

To demonstrate the grating as an all-optical tunable filter, we launched the TE-polarized pump light from a 980-nm laser diode (Lumentum, S27-7402-360-AL) and the TM-polarized signal light from the broadband source into the grating with a 980/1500 nm wavelength-division multiplexer (WDM), as shown in Fig. 4(a). Fig. 5(a) shows the transmission spectra of a grating with a pitch of 332 μm measured at different pump powers. As the pump power increases, the resonance wavelength shifts towards the shorter wavelength, which is consistent with the theoretical prediction. Fig. 5(b) shows the variation of the resonance wavelength with the pump power for three gratings, which have pitches 320, 326, and 332 μm, respectively. As expected, the grating with a shorter pitch has a shorter resonance wavelength. The tuning efficiencies of these grating are within –0.6 and –0.8 nm/mW. We should note that the pump power here refers to the output pump power from the input SMF. The fiber-waveguide coupling loss (~2.2 dB) reduces the pump power launched to the graphene film by ~40%. As pointed out earlier, the imperfections on the graphene film significantly reduces pump absorption. Excitation of high-order modes also reduce pump absorption. To directly measure the actual pump power absorbed by graphene, we compared the output pump powers measured for the TE and TM polarizations. We found that only ~16% of the input pump power was actually absorbed by graphene. Therefore, the expected tuning efficiency should be ~16% of the theoretical value, namely –4.5 nm/mW × 0.16 ≈ –0.7 nm/mW, which agrees well with our measurement result. It is possible to significantly increase the tuning efficiency by improving the quality of the graphene film, which can be

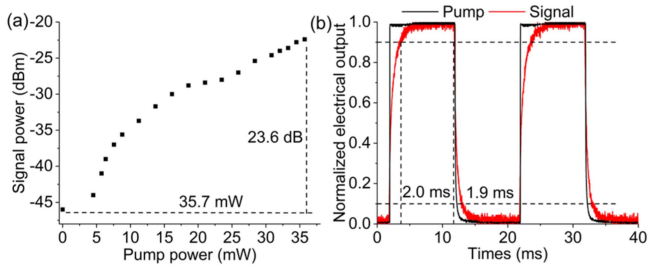

Fig. 6. (a) Variation of the output signal power with the input pump power at 1594.4 nm for the grating with a pitch of 332 μm, and (b) signal response times measured by switching the pump power between 0 mw and 35.7 mW.

realized by optimizing the graphene transfer method [28] or using double-layer graphene. Another way to increase pump efficiency is to use a longer pump wavelength, which can avoid excitation of high-order modes. As shown in Fig. 5(a), the bandwidth and the insertion loss do not change significantly with the pump power. While we present experimental results only for the TM polarization, all-optical tuning also works for the TE polarization, which, however, suffers from large absorption by the graphene film and hence a large insertion loss.

C. All-Optical Switching

Our grating can also function as an all-optical switch when operated at a fixed wavelength. To demonstrate the function of all-optical switching, we launched the TM-polarized signal light generated from the tunable laser and the TE-polarized pump light into the grating with a WDM. The signal wavelength was fixed at the resonance wavelength of the grating and the input signal power was fixed at –12.0 dBm. Fig. 6(a) shows the variation of the signal power with the pump power for the grating with a pitch of 332 μm. When the resonance wavelength is tuned away from its original value by increasing the pump power, the transmission at the original resonance wavelength increases. When the pump power reaches 35.7 mW, the signal power increases by 23.6 dB. In other words, by switching the pump power to 35.7 mW, the signal is switched on with an extinction ratio of 23.6 dB. The fiber-waveguide coupling loss and the propagation loss of the TM-polarized signal light were measured to be ∼1.5 dB/facet and ∼2.7 dB/cm, respectively. The low coupling loss allows our grating to be readily used in fiber-based systems.

We measured the response times of the switch by modulating the pump laser between 0 mW and 35.7 mW with a 50-Hz square-wave electrical signal generated from a function generator (GW Instek, AFG-2225) and detecting the output signals with a photodetector and an oscilloscope (MCP Lab Electronic, DQ8304C). As shown in Fig. 6(b), the rise and fall times of the switch are 2.0 ms and 1.9 ms, respectively, which are comparable with those obtained for other all-optical switches [23], [24] and electrically driven thermo-optic switches fabricated with polymer waveguides [21], [25]. The switching speed of our device are limited by the heat capacity and the thermal conductivity of the polymer waveguide. By optimizing heat transfer with improved waveguide design, it should be possible to increase the switching speed to several kHz [29]. We also measured the temperature sensitivity of the grating by varying the temperature of a semiconductor heater placed underneath. Our typical grating shows a temperature sensitivity of ∼2.8 nm/°C, which can be explored as a thermal tuning mechanism to extend the operation wavelength range of the grating. We should note that a change in the ambient temperature mainly affects the initial resonance wavelength; it does not significantly affect the tuning efficiency.

V. Conclusion

Thanks to graphene's large photothermal effect and strong polarization-dependent absorption, together with the merits of the polymer waveguide technology, low-power, low-loss all-optical tunable broadband filters have been realized with LPWGs formed in graphene-buried polymer waveguides. The wavelength-tuning efficiencies of our experimental gratings are approximately –0.7 nm/mW, which corresponds to a tuning range of ∼20 nm with a pump power lower than 30 mW. When operated as an all-optical switch, the grating can provide an extinction ratio higher than 20 dB with a pump power lower than 30 mW at a switching time of ∼2.0 ms. There is much room to further improve the performances of the gratings. Our gratings can be butt-coupled to fibers and pumped with CW light with little constraint on the pump wavelength. Given the flexibility in the design of LPWGs for achieving different functions [9], [10], [11], [12], [13], [14], [15], our grating platform opens up new opportunities for the development of advanced all-optical control devices for applications in both on-chip and fiber-based transmission systems.

References

[1] A. E. Willner et al., "All-optical signal processing techniques for flexible networks," *J. Lightw. Technol.*, vol. 37, no. 1, pp. 21–35, Jan. 2019.
[2] Z.-W. Li, Q. Liu, H. Wang, M. Deng, Q.-Z. Huang, and Y. Wang, "Photo-induced thermo-optical refraction switching by a graphene-assisted silicon microring resonator," *J. Lightw. Technol.*, vol. 39, no. 11, pp. 3471–3477, Jun. 2021.
[3] C. Qiu, Y. Yang, C. Li, Y. Wang, K. Wu, and J. Chen, "All-optical control of light on a graphene-on-silicon nitride chip using thermo-optic effect," *Sci. Rep.*, vol. 7, no. 1, 2017, Art. no. 17046.
[4] Y. Wang et al., "All-optical control of microfiber resonator by graphene's photothermal effect," *Appl. Phys. Lett.*, vol. 108, 2016, Art. no. 171905.
[5] T. Guo, S. Gao, H. Zeng, L. Tang, and C. Qiu, "All-optical control of a single resonance in a graphene-on-silicon nanobeam cavity using thermo-optic effect," *J. Lightw. Technol.*, vol. 39, no. 14, pp. 4710–4716, Jul. 2021.
[6] V. Rastogi and K. S. Chiang, "Long-period gratings in planar optical waveguides," *Appl. Opt.*, vol. 41, no. 30, pp. 6351–6355, 2002.
[7] Y.-B. Cho, B.-K. Yang, J.-H. Lee, J.-B. Yoon, and S.-Y. Shin, "Silicon photonic wire filter using asymmetric sidewall long-period waveguide grating in a two-mode waveguide," *IEEE Photon. Technol. Lett.*, vol. 20, no. 7, pp. 520–522, Apr. 2008.
[8] R. W. Chuang, M. T. Hsu, and G. S. Wang, "Long-period waveguide gratings with amorphous silicon cladding layer on silicon-on-insulator substrates realized by anisotropic wet etching," *Jpn. J. Appl. Phys.*, vol. 53, 2014, Art. no. 04EG15.
[9] Y. M. Chu, K. S. Chiang, and Q. Liu, "Widely tunable optical bandpass filter by use of polymer long-period waveguide gratings," *Appl. Opt.*, vol. 45, no. 12, pp. 2755–2760, 2006.
[10] Y. Bai, Q. Liu, K. P. Lor, and K. S. Chiang, "Widely tunable long-period waveguide grating couplers," *Opt. Exp.*, vol. 14, no. 26, pp. 12644–12654, 2006.
[11] W. Wang, J. Wu, K. Chen, W. Jin, and K. S. Chiang, "Ultra-broadband mode converters based on length-apodized long-period waveguide gratings," *Opt. Exp.*, vol. 25, no. 13, pp. 14341–14350, 2017.

[12] W. Jin and K. S. Chiang, "Leaky-mode long-period grating on a lithium-niobate-on-insulator waveguide," *Optica*, vol. 8, no. 12, pp. 1624–1631, 2021.
[13] J. Y. Deng, M. K. Wang, X. X. Ma, H. J. Li, J. Y. Wu, and K. X. Chen, "Spot-size converter based on long-period grating," *IEEE Photon. J.*, vol. 14, no. 2, Apr. 2022, Art. no. 6620205.
[14] W. Zhao, J. Feng, K. Chen, and K. S. Chiang, "Reconfigurable broadband mode (de)multiplexer based on an integrated thermally induced long-period grating and asymmetric Y-junction," *Opt. Lett.*, vol. 43, no. 9, pp. 2082–2085, 2018.
[15] W. Jin and K. S. Chiang, "Reconfigurable three-mode converter based on cascaded electro-optic long-period gratings," *IEEE J. Sel. Topics Quantum Electron.*, vol. 26, no. 5, Sep./Oct. 2020, Art. no. 4500906.
[16] B. J. Eggleton, R. E. Slusher, J. B. Judkins, J. B. Stark, and A. M. Vengsarkar, "All-optical switching in long-period fiber gratings," *Opt. Lett.*, vol. 22, no. 12, pp. 883–885, 1997.
[17] H. C. Nguyen et al., "Nonlinear long-period gratings in As_2Se_3 chalcogenide fiber for all-optical switching," *Appl. Phys. Lett.*, vol. 92, 2008, Art. no. 101127.
[18] Z. Chang and K. S. Chiang, "Experimental verification of optical models of graphene with multimode slab waveguides," *Opt. Lett.*, vol. 41, no. 9, pp. 2129–2132, 2016.
[19] Z. Chang and K. S. Chiang, "Ultra-broadband mode filters based on graphene-embedded waveguides," *Opt. Lett.*, vol. 42, no. 19, pp. 3868–3871, 2017.
[20] Q. Huang and K. S. Chiang, "Polarization-insensitive ultra-broadband mode filter based on a 3D graphene structure buried in an optical waveguide," *Optica*, vol. 7, no. 7, pp. 744–745, 2020.
[21] X. Wang, W. Jin, Z. Chang, and K. S. Chiang, "Buried graphene electrode heater for a polymer waveguide thermo-optic device," *Opt. Lett.*, vol. 44, no. 6, pp. 1480–1483, 2019.
[22] Z. Chang and K. S. Chiang, "All-optical loss modulation with graphene-buried polymer waveguides," *Opt. Lett.*, vol. 44, no. 15, pp. 3685–3688, 2019.
[23] L. Jiang, Q. Huang, and K. S. Chiang, "Low-power all-optical switch based on a graphene-buried polymer waveguide Mach-Zehnder interferometer," *Opt. Exp.*, vol. 30, no. 5, pp. 6786–6797, 2022.
[24] L. Jiang and K. S. Chiang, "All-optical mode switching with a graphene-buried polymer waveguide directional coupler," *Opt. Lett.*, vol. 47, no. 10, pp. 2414–2417, 2022.
[25] X. Wang and K. S. Chiang, "Polarization-insensitive mode-independent thermo-optic switch based on symmetric waveguide directional coupler," *Opt. Exp.*, vol. 27, no. 24, pp. 35385–35393, 2019.
[26] A. M. Vengsarkar, P. J. Lemaire, J. B. Judkins, V. Bhatia, T. Erdogan, and J. E. Sipe, "Long-period fiber gratings as band-rejection filters," *J. Lightw. Technol.*, vol. 14, no. 1, pp. 58–65, Jan. 1996.
[27] A. A. Balandin et al., "Superior thermal conductivity of single-layer graphene," *Nano Lett.*, vol. 8, no. 3, pp. 902–907, 2008.
[28] H. Park et al., "Optimized poly(methyl methacrylate)-mediated graphene-transfer process for fabrication of high-quality graphene layer," *Nanotechnology*, vol. 29, 2018, Art. no. 415303.
[29] Q. Xu et al., "Fast and low-power thermo-optic switch based on organic-inorganic hybrid strip-loaded waveguides," *Opt. Lett.*, vol. 43, no. 20, pp. 5102–5105, 2018.